



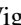


Spin-charge separation in the quantum boomerang effect

Pablo Capuzzi ^{1,2}, Luca Tessieri ³, Zehra Akdeniz ⁴, Anna Minguzzi ⁵, and Patrizia Vignolo ^{6,7}

¹*Departamento de Física, Facultad de Ciencias Exactas y Naturales, Universidad de Buenos Aires, Pabellón 1, Ciudad Universitaria, 1428 Buenos Aires, Argentina*

²*Instituto de Física de Buenos Aires (UBA-CONICET), Pabellón 1, Ciudad Universitaria, 1428 Buenos Aires, Argentina*

³*Instituto de Física y Matemáticas, Universidad Michoacana de San Nicolás de Hidalgo, 58060 Morelia, Mexico*

⁴*Faculty of Science and Letters, Piri Reis University, 34940 Tuzla, Istanbul, Turkey*

⁵*Université Grenoble Alpes, CNRS, LPMMC, 38000 Grenoble, France*

⁶*Université Côte d'Azur, CNRS, Institut de Physique de Nice, 06200 Nice, France*

⁷*Institut Universitaire de France, France*



(Received 8 April 2024; accepted 23 May 2024; published 10 June 2024)

We study the localization dynamics of a SU(2) fermionic wave packet launched in a (pseudo)random potential. We show that, in the limit of strong intercomponent repulsions, the total wave packet exhibits a boomeranglike dynamics, returning to near its initial position as expected for noninteracting particles, while separately each spin-component does not. This spin-charge separation effect occurs both in the infinite repulsive limit and at finite interactions. At infinite interactions, the system is integrable and thermalization cannot occur: the two spin-components push each other during the dynamics and their centers of mass stop further from each other than their initial positions. At finite interactions, integrability is broken, the two spin-components oscillate and mix, with their center-of-mass positions converging very slowly to the center of mass of the whole system. This is a signature that the final localized state is a fully spin-mixed thermalized state.

DOI: [10.1103/PhysRevA.109.063315](https://doi.org/10.1103/PhysRevA.109.063315)

I. INTRODUCTION

In disordered quantum systems it has been shown that a wave packet launched with some initial velocity may return to its initial position and stop there. This phenomenon, known as the quantum boomerang effect (QBE) [1–3], occurs in the Anderson localization (AL) limit when interactions are completely negligible and disorder completely freezes the dynamics of the wave packet [4,5]. The QBE is found not only in real space, but also in momentum space. In this latter case, the (pseudo)disorder in momentum space is introduced by kicking periodically the wave packet. Indeed, the first experimental evidence of the QBE was obtained in a quantum kicked-rotor experiment [3]. These measurements have confirmed the theoretical predictions [1,2] and elucidated the crucial role of the time-reversal symmetry in determining the presence or absence of the QBE. In fact, the occurrence of the QBE requires not only that the system be in the AL regime but also that some symmetries of the Hamiltonian and of the initial state of the wave packet be fulfilled [6–8]. When localization takes place in momentum space, as in the case of the kicked rotor, it is the time-reversal symmetry that is crucial for the wave packet to come back to its initial position. On the other hand, for systems that localize in real space, like the Anderson model, it is the space-time reversal symmetry that regulates the dynamics of the quantum boomerang [6,8]. When this symmetry is broken, the wave packet—after having been launched—stops somewhere but not necessarily in its initial position.

Like Anderson localization, the QBE is a phenomenon that is expected for noninteracting systems, both bosonic and

fermionic. It has been shown that weak interactions between particles partially destroy the QBE: the center of mass of the wave packet makes a U-turn, but without coming back to its initial position [9]. This also happens for a one-dimensional (1D) strongly interacting Bose gas, which can be mapped to a weakly interacting Fermi gas [10]: interactions partially destroy interference effects and thus the QBE. However, in the limit where the interactions are infinitely repulsive, namely, in the Tonks-Girardeau regime, the QBE holds since the system can be mapped onto free fermions [10].

In this paper, we investigate the quantum boomerang dynamics of a strongly repulsive two-component Fermi gas (see Fig. 1). The underlying idea is to explore a system where different spin configurations are available and study if the QBE, or its failure, can bring information about the thermalization of the system and, possibly, whether its final state is many-body localized [11–13].

A two-component Fermi gas with strong, repulsive intercomponent contact interactions can be mapped onto an effective spin-chain Hamiltonian where the spins exchange when particles of different spin-components collide [14]. The dynamics of such a system starting from an initially spin-demixed configuration have been studied in the absence of disorder [15–17], highlighting that the short-time superdiffusive dynamics of the magnetization interface for two spin-components happens in a similar way in spin chains [18–21]. It has also been shown that such a system relaxes towards the microcanonical ensemble during a time interval that increases with the number of particles, integrability being broken by the presence of an external potential at finite interactions [17].

The presence of the disorder localizes the whole wave packet as well as the two spin-components. The size of the wave packet for each spin-component is initially half of the total size, but very rapidly the two spin-components mix so that their size quickly reaches that of the total wave packet. Simultaneously, the center of mass of the whole system does a U-turn and stops at its initial position, as if the system were noninteracting. Instead, the center of mass of each spin-component does not return to its initial position but, in the presence of finite interactions, converges towards the position of the center of mass of the whole system, with a damped oscillating dynamics much slower than that of the whole density. This separation of timescales is due to the fact that the spin dynamics is governed by the inverse of the interaction strength, which is very large in our model. We therefore observe a charge-spin separation in the QBE.

Moreover, at finite interactions, where spin mixing occurs, we find that the final localized spin densities are those expected in the microcanonical ensemble, whereas, in the limit of infinite interaction strength, where the centers of mass of two spin-components stop further apart from their initial positions, the final localized state is very different from that expected in the microcanonical ensemble because integrability prevents thermalization.

The manuscript is organized as follows. The physical model is introduced in Sec. II, where we remind how the system can be mapped onto a spin-chain model and the dynamics can be exactly solved in the strong-interacting limit. Then, the boomerang experiment is described in Sec. III, where we detail a proposal for an experimental protocol and analyze the results, discussing the role of the interactions and of the symmetries. The thermalization issue is discussed in Sec. IV. Concluding remarks are given in Sec. V.

II. THE MODEL

We consider a SU(2) fermionic mixture with $N_\uparrow(N_\downarrow) = N/2$ fermions in the spin-up (spin-down) component. Each fermion is subject to an external potential $V(x)$ and interacts with fermions of the other spin component via a repulsive contact potential of strength g . Thus, the many-body Hamiltonian reads

$$\mathcal{H} = \mathcal{H}_0 + \sum_{i=1}^{N_\uparrow} \sum_{j=N_\uparrow+1}^N g \delta(x_i - x_j), \quad (1)$$

with

$$\mathcal{H}_0 = \sum_{i=1}^N \left[-\frac{\hbar^2}{2m} \frac{\partial^2}{\partial x_i^2} + V(x_i) \right]. \quad (2)$$

Close to the fermionized regime, where interactions are so large that they play the role of a Pauli principle between fermions belonging to different spin components, the many-body wave function can be written as [22]

$$\Psi(X) = \sum_{P \in S_N} a_P \theta_P(X) \Psi_A(X), \quad (3)$$

where the summation is performed over all P permutations of N elements, S_N . The vector $X = (x_{1,\sigma_1}, \dots, x_{N,\sigma_N})$ includes

particle coordinates x_i and spin indices σ_i , $\Psi_A(X; t)$ is the zero-temperature solution for spinless fermions obeying the noninteracting Hamiltonian \mathcal{H}_0 , and $\theta_P(X)$ is the generalized Heaviside function, which is equal to 1 in the coordinate sector $x_{P(1),\sigma_{P(1)}} < \dots < x_{P(N),\sigma_{P(N)}}$ and 0 otherwise. The coefficients a_P are determined by minimizing the energy [22]:

$$E = E_\infty + \frac{1}{g} \left(\frac{\partial E}{\partial g^{-1}} \right)_{1/g \rightarrow 0} = E_\infty - \frac{\mathcal{C}}{g}, \quad (4)$$

where E_∞ is the energy in the fully fermionized regime and $\mathcal{C} = -(\partial E / \partial g^{-1})_{1/g \rightarrow 0}$ is Tan's contact up to a dimensional constant. This is equivalent to solving the eigenvalue problem of the effective Hamiltonian

$$\mathcal{H}_{\text{eff}} = \mathcal{H}|_{1/g \ll 1} = E_\infty \hat{1} + H_S \quad (5)$$

obtained by expanding \mathcal{H} on the $\{\phi_n\}$ snippet basis, namely, the basis of all particle sectors obtained by global permutations modulo the permutations of identical fermions with the same spin [23]. Furthermore, it has been shown that H_S is equivalent to a spin-chain Hamiltonian in position particle space [14],

$$H_S = \sum_{j=1}^{N-1} (-J_j \hat{1} + J_j \hat{P}_{j,j+1}), \quad (6)$$

where $\hat{P}_{j,j'} = (\vec{\sigma}^{(j)} \vec{\sigma}^{(j')} + 1)/2$ is the permutation operator and $\vec{\sigma}^{(j)} = (\sigma_x^{(j)}, \sigma_y^{(j)}, \sigma_z^{(j)})$ are the Pauli matrices. The hopping terms J_j in Eq. (6) can be written as

$$J_j = \frac{N!}{g} \int_{-\infty}^{\infty} dX \delta(x_i - x_{i+1}) \theta_{\text{id}}(X) \left| \frac{\partial \Psi_A}{\partial x_i} \right|^2. \quad (7)$$

A. The dynamics close to the fermionized regime

In an out-of-equilibrium situation, when the free-fermion part of the wave function Ψ_A is time dependent, the J_j terms (7) change in time. Therefore, to obtain $\Psi(X, \bar{t} + dt)$ starting from $\Psi(X, \bar{t})$, we proceed as follows [24]. We start by finding $J_j(\bar{t})$ to determine the spin-chain Hamiltonian at a time \bar{t} . By diagonalizing $H_S(\bar{t})$ we obtain the eigenvectors $a_P^{(j)}(\bar{t})$ and their corresponding eigenvalues $\mathcal{E}_j(\bar{t})$. Expanding the coefficients a_P of Eq. (3) in this basis gives the identity $a_P(\bar{t}) = \sum_j \alpha_j(\bar{t}) a_P^{(j)}(\bar{t})$ and makes it possible to compute the coefficients at a time $\bar{t} + dt$ as

$$a_P(\bar{t} + dt) = \sum_j \alpha_j(\bar{t}) e^{-i\mathcal{E}_j(\bar{t})dt/\hbar} a_P^{(j)}(\bar{t}). \quad (8)$$

Once the evolved coefficients (8) are known, the many-body wave function at a time $\bar{t} + dt$ can be written as

$$\Psi(X; \bar{t} + dt) = \sum_{P \in S_N} a_P(\bar{t} + dt) \theta_P(X) \Psi_A(X; \bar{t} + dt). \quad (9)$$

For this approach to work, the time steps need to fulfill the condition $dt \ll \hbar/|J_j(\bar{t} + dt) - J_j(\bar{t})|$ for any \bar{t} and any j . Once the many-body wave function is calculated, we can compute the spin densities at each time:

$$\rho_{\uparrow,\downarrow}(x, t) = \sum_i \delta_{\sigma_i}^{\uparrow,\downarrow} \sum_{P \in S_N} |a_P(t)|^2 \rho^i(x, t), \quad (10)$$

where $\delta_{\sigma_i}^\uparrow$ ($\delta_{\sigma_i}^\downarrow$) is the Kronecker delta for spin σ_i and \uparrow (\downarrow) and

$$\rho^i(x, t) = \int_{x_1 < \dots < x_{i-1} < x < x_{i+1} < \dots < x_N} dX \delta(x - x_i) |\Psi_A(X, t)|^2$$

is the density in the sector $x_1 < \dots < x_{i-1} < x < x_{i+1} < \dots < x_N$, while the total density is $\rho(x, t) = \sum_{i=1}^N \rho_i(x, t) = \rho_\uparrow(x, t) + \rho_\downarrow(x, t)$.

B. The dynamics in the presence of disorder

We now focus our attention on the case of a wave packet of fermions initially prepared at equilibrium in a harmonic trap of frequency ω , which is then released with an imprinted initial momentum $\hbar k_0$ on each fermion and propagates in the pseudorandom potential

$$V_{\text{dis}}(x) = \mathcal{W} \sin(\sqrt{5}\pi(x + i_c L/2)/(a_{\text{ho}}/10)^3) \quad (11)$$

where \mathcal{W} is the potential amplitude, $a_{\text{ho}} = \sqrt{\hbar/(m\omega)}$ is the typical harmonic potential length scale, L is the size of the system, and i_c is an integer index that counts the pseudodisorder configurations. It has already been shown that the potential (11), defined on a lattice, induces both Anderson localization [25] and the boomerang effect [2] as a truly random potential. We choose the potential (11), rather than a truly random one, because of its relevance to cold-atom experiments, in which pseudorandom potentials can be realized with appropriate laser configurations [26]. We would like to stress, however, that we have verified that the results described in this paper are still valid if the pseudorandom potential (11) is replaced with a random potential of adequate strength [2]. The potential (11) has zero average $\overline{V_{\text{dis}}(x)} = 0$ and is δ -correlated, $\overline{V_{\text{dis}}(x)V_{\text{dis}}(x')} = \gamma\delta(x - x')$. The values obtained from Eq. (11) by keeping x fixed and varying i_c have a uniform probability distribution function (PDF). Here and in the rest of this paper, we use the symbol $\langle \dots \rangle$ to denote the average over a sequence of pseudodisorder configurations [we consider different i_c values in Eq. (11)].

The disorder strength γ determines the mean-free path ℓ and the mean-free time τ for a noninteracting system. Indeed, we remind that for a wave packet with the momentum $\hbar k_0$ in the Born approximation, one has [1]

$$\ell = \frac{\hbar^4 k_0^2}{2m^2 \gamma} \quad \text{and} \quad \tau = \frac{\hbar^3 k_0}{2m\gamma}. \quad (12)$$

Here and in the following, we have fixed $\gamma = 0.86 \times 10^3 \hbar^2 \omega^2 a_{\text{ho}}$ and $k_0 = 50/a_{\text{ho}}$, which imply that $\ell = 1.45 a_{\text{ho}}$ and $\tau = 0.029 \omega^{-1}$. We remark that, in order to use such expressions for the case of N noninteracting fermions, $(\hbar k_0)^2/(2m)$ has to be much larger than the energy of the highest occupied orbital [10], namely, the Fermi energy of the system.

The presence of disorder significantly influences the time evolution of the hopping terms J_i . In an experiment in which the wave packet is first prepared separately in a deterministic initial condition and then left to evolve in a disordered potential, the J_i 's at time $t = 0$ are determined by the initial state and their PDFs are Dirac δ 's [as shown in Fig. 2(a)]. Because the fermions move in a (pseudo)random potential, the hopping terms become stochastic variables, with disorder

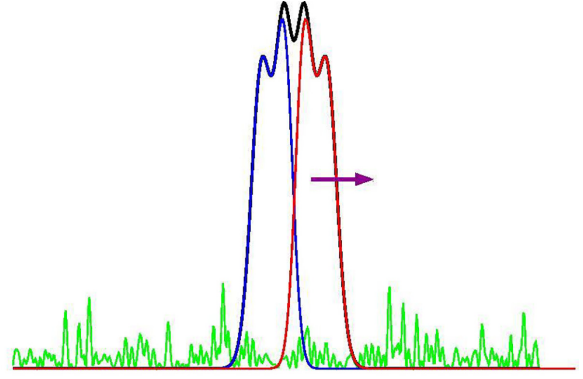


FIG. 1. Schematic representation of the system studied in this work: a spatially spin-demixed initial state is realized with an initial nonvanishing momentum in a disorder potential.

entering via the time evolution of Ψ_A . As a consequence, at each time t , the statistical properties of the J_i terms must be described with a PDF $P(J_i)$. The time evolution of the corresponding marginal PDFs is depicted in Fig. 2, which shows that initially the PDFs broaden and drift towards higher values of J_i , eventually reaching stable asymptotic forms at longer times. These qualitative features are evinced by the time evolution of the average values of the J_i 's and of their rescaled standard deviations

$$\frac{\sigma_{J_i}}{\bar{J}_i} = \frac{\sqrt{\bar{J}_i^2 - \bar{J}_i^2}}{\bar{J}_i}, \quad (13)$$

as shown in Fig. 3.

We can estimate the dependence of the mean-free path ℓ_j and of the mean-free time τ_j on \bar{J}_i and σ_{J_i} for the spin dynamics by using the expression for the localization length for a lattice system with random off-diagonal disorder, derived

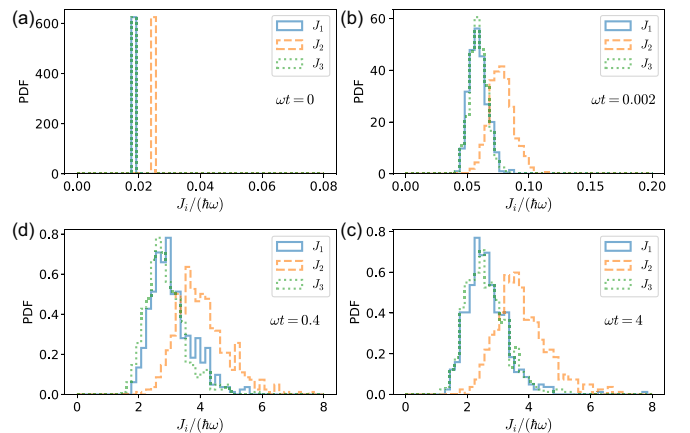


FIG. 2. Evolution of PDFs of the J_i terms for the case of an initial deterministic wave packet of $2 + 2$ fermions, initially prepared in a harmonic trap of frequency ω , launched with an initial momentum $\hbar k_0$ in the presence of a pseudorandom potential (11). The different panels correspond to the following times: (a) 0, (b) 0.002, (c) 0.4, and (d) 4, in units of $1/\omega$. Note that in panel (a), corresponding to the initial state, the PDFs of J_1 and J_3 are the same.

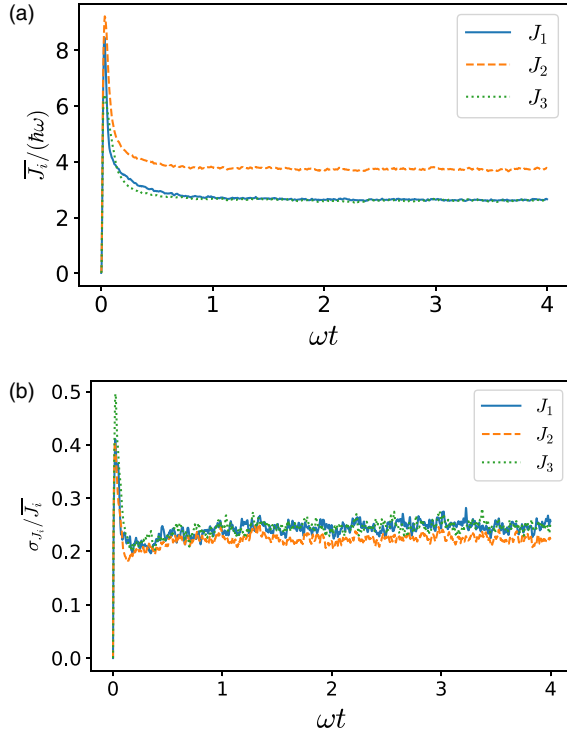


FIG. 3. Average hopping terms \bar{J}_i , for the case $g = 100\hbar\omega a_{\text{ho}}$, (a) and relative standard deviation (13) of the hopping terms J_i (b), as functions of time, for the same experimental protocol as for Fig. 2 and described in Sec. III.

in the Born approximation [2]. This would give

$$\ell_j \propto \frac{\bar{J}_i^2}{\sigma_{J_i}^2}, \quad \text{and} \quad \tau_j \propto \frac{\bar{J}_i}{\sigma_{J_i}}. \quad (14)$$

Equations (14) predict that ℓ_j does not depend on the strength of the interactions g , whereas τ_j increases with it ($\tau_j \propto g$), which is in agreement with the results presented in the next section.

Finally, let us discuss the stochastic properties of the $J_i(t)$'s. They are ultimately shaped by the random potential $V_{\text{dis}}(x)$, but, unfortunately, the determinantal form of Ψ_A makes it highly nontrivial to establish a link between the randomness of the potential $V_{\text{dis}}(x)$ and the stochastic features of the J_i terms. As shown by Eq. (7), the magnitude of the J_i 's is proportional to the sharpness of the cusps, namely, the slope of the wave function $\Psi_A(X)$ when two particles approach each other. Therefore, we expect that their average values should strongly depend on the specific features of the experimental protocol.

In the present case, we consider a wave packet launched with an initial momentum in a disordered landscape. Our numerical analysis has shown that the marginal PDFs of the J_i terms tend to asymptotic forms characterized by a skewed shape and fat tails.

III. THE BOOMERANG DYNAMICS

We propose in this section an experimental protocol to observe QBE. We consider an initially spatial phase-separated

SU(2) fermionic mixture with $N_\uparrow = N_\downarrow$ where the up spins are on the left (L) and the down spins are on the right (R), both trapped in the harmonic potential $V_{\text{ho}} = m\omega^2 x_i^2/2$. At $t = 0$ we release the fermions in the disorder potential $V_{\text{dis}}(x_i)$ by kicking them towards the right with an initial momentum $\hbar k_0$ and switching off the harmonic potential.

We study the dynamics of the center-of-mass \bar{x} and the width w of the total disordered-averaged density profile,

$$\bar{x} = \int \bar{\rho}(x) x dx / N, \quad (15)$$

$$w = \left(\int \bar{\rho}(x) (x - \bar{x})^2 dx / N \right)^{1/2}, \quad (16)$$

and we do the same for each spin component,

$$\bar{x}_{\uparrow,\downarrow} = \int \bar{\rho}_{\uparrow,\downarrow}(x) x dx / N_{\uparrow,\downarrow}, \quad (17)$$

$$w_{\uparrow,\downarrow} = \left(\int \bar{\rho}_{\uparrow,\downarrow}(x) (x - \bar{x}_{\uparrow,\downarrow})^2 dx / N_{\uparrow,\downarrow} \right)^{1/2}. \quad (18)$$

Note that to simulate such an experimental protocol in the procedure detailed in Sec. II, the time discretization needs to verify $dt < \tau$.

A. Spin-charge separation in the boomerang dynamics

We observe (see Fig. 4) that, in the fermionized regime ($g \rightarrow \infty$), the two components never mix, and they localize independently, repelling each other. Indeed, in this case the hopping terms J_i vanish and

$$\rho_\uparrow^\infty(x, t) = \rho^L(x, t) = \sum_{i=1}^{N_\uparrow} \rho^i(x, t) \quad (19)$$

and

$$\rho_\downarrow^\infty(x, t) = \rho^R(x, t) = \sum_{i=N_\uparrow+1}^N \rho^i(x, t). \quad (20)$$

Moreover, the width of each component is half of the width of the total density, and we observe that the final position of the center of mass of each spin-component is $\bar{x}_{\uparrow,\downarrow}^\infty(t \rightarrow \infty) \simeq \pm w/2$.

The dynamical behavior is considerably different when interactions are large but finite: in this case the two spin-components undergo mixing during the dynamics, as happens in the absence of the disorder [17] (see Fig. 4). Each spin-component is localized by the disordered hoppings, reaching a final width that is the same of the two components [Fig. 4(a)]. Initially, each component moves away over a distance ℓ_{max} , and then it comes back towards the initial position of the center of mass of the whole system, performing damped oscillations, around this position. These oscillations are governed by the frequency spectrum of the spin-chain Hamiltonian (6), which yields the lowest nonzero frequency $\omega^* = (J_1 + J_2 - \sqrt{J_1^2 + J_2^2})/\hbar$, where we have used that at long times $J_1 = J_3$. As shown in Fig. 4(b), the turning point ℓ_{max} is roughly the same for the cases $g/(\hbar\omega a_{\text{ho}}) = 100$ and 200, and the time evolution scales with g , namely, $\bar{x}_{\uparrow,\downarrow}(2t)_{2g} \simeq \bar{x}_{\uparrow,\downarrow}(t)_g$, as predicted by Eqs. (14). The localization dynamics of each

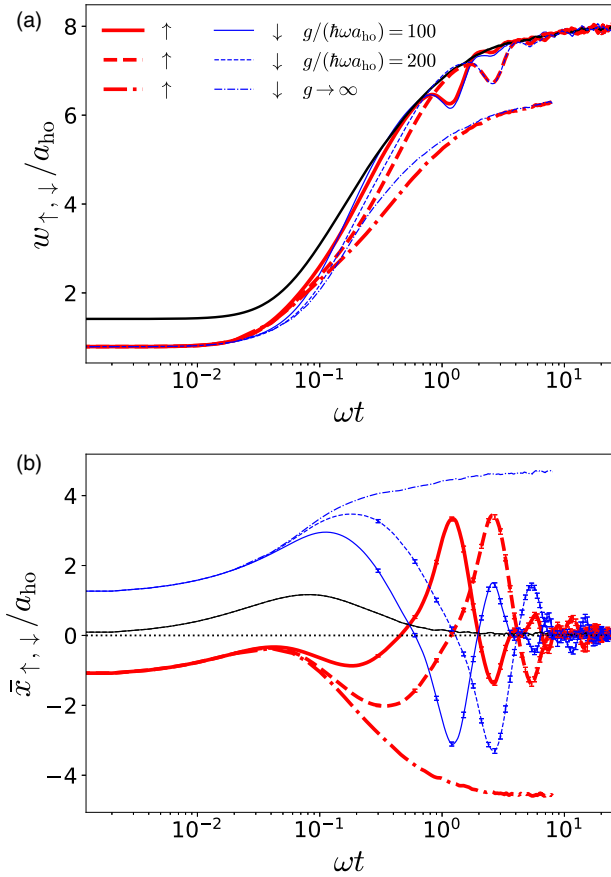


FIG. 4. Disorder-averaged widths w (a) and center-of-mass positions (b) \bar{x} of the whole system (black solid lines) and of each spin component (red thick and blue thin lines) as functions of time (in logscale), for different values of the interaction strengths: $g/(\hbar\omega a_{ho}) = 100$ (continuous lines), $g/(\hbar\omega a_{ho}) = 200$ (dashed lines), and $g \rightarrow \infty$ (dot-dashed lines). Here we used the following parameters: $k_0 a_{ho} = 50$, $\gamma = 0.86 \times 10^3 \hbar^2 \omega^2 a_{ho}$, and $N = 4$ and we averaged over 512 configurations.

spin-component occurs on a much longer timescale with respect to that of the total density. In particular, we observe that at long times one has

$$\bar{x}_{\uparrow, \downarrow} = \frac{1}{2}(\bar{x}_{\uparrow}^{\infty} + \bar{x}_{\downarrow}^{\infty}) \pm \frac{1}{2}(\bar{x}_{\uparrow}^{\infty} - \bar{x}_{\downarrow}^{\infty})\mathcal{F}(t), \quad (21)$$

with $\mathcal{F}(t)$ being a function that depends on the average of spin weights only, $|a_P(t)_i|^2 \delta_{\sigma_i}^{\uparrow, \downarrow}$. Indeed, the timescales of the density dynamics and of the spin dynamics being very different (the first being determined by the disorder strength γ and the second by the hoppings J_i that are proportional to ρ^3/g [27,28]), the average over configurations splits into two independent parts as if the two dynamical processes were uncorrelated (see the Appendix).

The center of mass of the total density, depicted in Fig. 4(b), exhibits the boomerang dynamics: the whole wave packet moves away over a distance of $\sim \ell$ and then comes back to its initial position, while at the same time the wave packet localizes. However, each spin-component individually does not come back to its initial position, but its center-of-mass position at long times coincides with the center of mass of the whole system.

Note that the behavior of the total density does not depend on the value of the interaction strength in the regime we are analyzing ($1/g \ll 1$), so that the black curves in Fig. 4 concern the three cases analyzed [$g/(\hbar\omega a_{ho}) = 100, 200, \infty$], indeed both the cases of $g = 100$ and $g = 200$ make it clear that increasing the interaction slows down the spin dynamics but does not alter the behavior of the center of mass of the whole system. We thus observe a spin-charge separation with respect to the boomerang dynamics, for both finite and infinite values of the interaction strength. This result is in agreement with the prediction of spin-charge separation in the localization dynamics for a disordered chain of spin-1/2 fermions [12].

B. Role of the interactions and symmetries

A straightforward interpretation of our results is the following one. In the strongly interacting mixture, the whole density is described by the spinless-fermions solution. Thus, the whole density follows the boomerang dynamics as expected for noninteracting fermions or Tonks-Girardeau bosons [10]. The effect of the interactions manifests itself in the inter-spin-component dynamics, but in a very different way depending on whether the interactions are infinite or finite. When the interactions are infinite, each spin-component is just a system of noninteracting particles that is not free to propagate everywhere because of the presence of the other component. It localizes at the same time as the whole system, but largely far away from the position of the center of mass of the whole system and also largely far away from their initial position. The center of mass of each component does not do the boomerang dynamics: each component moves away but does not come back because it is pushed by the other component.

Instead, when the interaction is large but finite, the situation is completely different. The landscape of the disorder felt by the spins completely changes. Particles with different spin hop with a spatially random probability, which fluctuates as a function of time and is inversely proportional to the interaction strength. The center of mass of each component reaches a final position that is different from the initial one, as already found for other interacting systems [10], and coincides with that of the whole system.

From the point of view of each component, there is an initial time when the dynamics at finite interactions coincides with that at infinite interactions, but then the trajectories separate, one going back while the other does not. This is very different from what happens with a single-component system [10] where the center of mass for the gas of finite interactions slightly deviates from that with infinite interactions.

As a final remark, we would like to highlight the role of symmetries for the QBE. As pointed out in Refs. [6,8], the QBE takes place in real space if the ensemble of the disordered Hamiltonians $\{\mathcal{H}\}$ is invariant under the action of \mathcal{RT} and if the initial state is an eigenstate of \mathcal{RT} , where \mathcal{R} is the spatial reversal operator and \mathcal{T} is the time-reversal operator. For the system we have considered in this work, both conditions are fulfilled. However, each spin-component is *not* an eigenstate of \mathcal{RT} . Under the action of \mathcal{RT} the spin-up component on the left is transformed on the spin-down component on the right, and vice versa. Thus, each

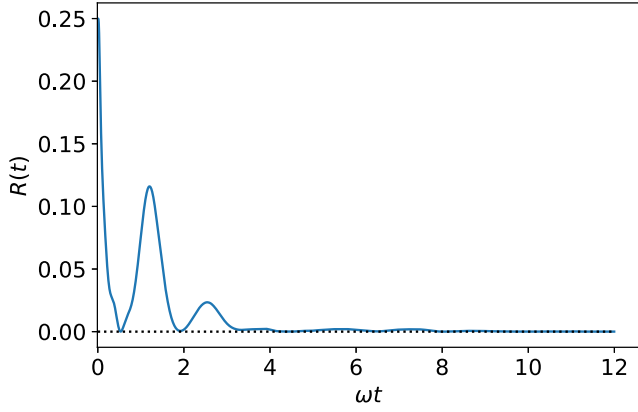


FIG. 5. Distance $R(t)$ from the spin part of the time-dependent average spin density $\bar{\rho}_\uparrow(t)$ to the microcanonical one $\rho_{\uparrow,MC}$ as function of time t .

spin-component separately does not fulfill the condition for the QBE, but the two spin-components system does.

IV. THE THERMALIZATION ISSUE

Given that the system we are studying is characterized by interactions and disorder, it is natural to ask whether the final localized state is many-body localized or if the eigenstate thermalization hypothesis (ETH) holds. In the latter case, the expectation values of local operators will ultimately evolve in time to their values predicted by the microcanonical ensemble [17,29]. Such a target state, for our system, coincides with a state described by the diagonal ensemble where the spin densities $\rho_{\uparrow,MC}(x)$ and $\rho_{\downarrow,MC}(x)$ are equally distributed. Of course, this cannot happen at infinite interactions: in this limit the system is integrable and the different spins, which are initially spatially phase separated, never mix, making it impossible to achieve a uniform nonmagnetized state. But at large finite interactions, even if slowly, the spin mixing takes place and continues even after the total density has localized. The long-time position of the center of mass of each spin-component coincides with the position of the center of mass of the whole localized cloud. This is in accordance with what one would expect with the aforesaid fully mixed state where $\rho_{\uparrow,MC}(x) = \rho_{\downarrow,MC}(x)$. Furthermore, since we have verified that the particle densities $\rho^i(x, t)$ and the amplitudes $|[a_P(t)]_i|^2$ entering the spin densities [cf. Eq. (10)] possess different relaxation times, in order to investigate the thermalization of the spin dynamics we have evaluated the distance

$$R(t) = \sum_i \left(\sqrt{\sum_{P \in \mathcal{S}_N} |[a_P(t)]_i|^2} - \sum_{P \in \mathcal{S}_N} |[a_P]_i^{MC}|^2 \right), \quad (22)$$

where $[a_P]_i^{MC}$ are the coefficients obtained from the diagonal ensemble, analogously to what has been done in Ref. [17] (see Fig. 5). With $R(t)$ collapsing to 0 very rapidly, it is clear that, for what concerns the spin density distributions, our system is consistent with the ETH. Thermalization was also reported for spin chains subject to off-diagonal disorder [30]. Our case displays some differences with the above, as the effective disorder felt by the spins is time dependent, as it originates

from the dynamics of the orbital part. It is also interesting to mention that the disorder felt by the particles is diagonal, but it turns off-diagonal as felt by the spins because it is mediated by the interaction among particles.

In conclusion, we would like to emphasize that the center-of-mass evolution of the spin components, namely, whether the boomerang dynamics occurs for the spin components, is an experimentally accessible tool to probe the lack of thermalization and the compatibility with the ETH.

V. CONCLUDING REMARKS

In this work we have studied the dynamics of a two-component fermionic wave packet launched in a 1D pseudorandom potential. We have considered the case of initially spatially phase-separated fermions characterized by strong, repulsive interspecies contact interactions. In such a strongly interacting limit, the charge and the spins dynamics decouple. The total density coincides with the total density of a noninteracting spinless Fermi gas, while the spin components obey an effective nonhomogeneous Heisenberg spin-chain Hamiltonian, whose hopping terms, which depend on the density evolution, become random during the dynamics and fluctuate in time. As a result, we find that the total density performs a boomerang dynamics as predicted for noninteracting particles, while the densities of each spin-component, considered separately, do not. Their centers of mass initially move away and then they come back, not to their respective initial position, but towards the initial position of the whole system. They reach this position, making damped oscillations, whose frequency is determined by averages of the effective hopping energy. The two spin-components mixed together reach a final spin-density distribution that is compatible with that of the diagonal (microcanonical) ensemble. This is a signature that interactions, in our system, do not induce many-body localization, at least for the parameters that we have chosen for our study. This result is reminiscent of previous studies [29] that have shown that for a Heisenberg spin chain with off-diagonal quenched disorder, many-body localization does not occur. Finally, let us underline that the system we have studied in this work opens up the possibility to realize, with an ultracold atom experiment, a quantum simulator of a Heisenberg spin chain with off-diagonal disorder. However, our system differs from that analyzed in Refs. [31–34] as the spatial part is subject to a diagonal disorder and the spin components feel an off-diagonal time-dependent disorder. This could bring unexpected novel phases and deserves further studies for larger systems, correlated disorder, and finite temperature.

ACKNOWLEDGMENTS

The authors acknowledge the CNRS International Research Project COQSYS for their support, funding from Grant No. ANR-21-CE47-0009 of the Quantum-SOPHA project, support of the Institut Henri Poincaré (UAR 839 CNRS-Sorbonne Université) and LabEx CARMIN (Grant No. ANR-10-LABX-59-01), and support from the Scientific Research Fund of Piri Reis University under Project No. BAP-2024-04. P.C. acknowledges support from CONICET (Consejo Nacional de Investigaciones Científicas y

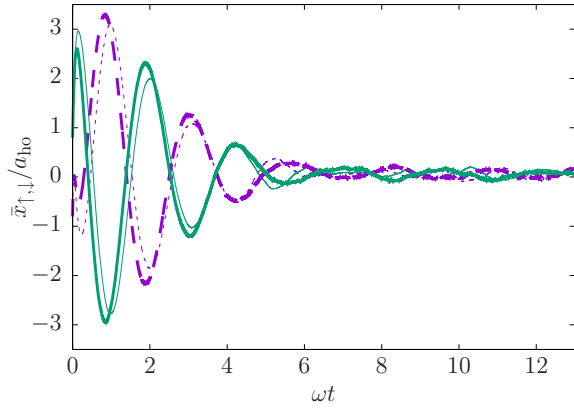


FIG. 6. Spin-up (violet dashed lines) and spin-down (green solid lines) center-of-mass positions \bar{x}_{\uparrow} and \bar{x}_{\downarrow} in units of a_{ho} as functions of the time t , for the case of a two-particle systems. The exact results (thick lines) are compared with those obtained using Eq. (A5).

Técnicas) under Grant No. PIP 11220210100821CO and Universidad de Buenos Aires under Grant No. UBACyT 20020220100069BA. L.T. acknowledges the financial support of the CIC-UMSNH under Grant No. 18090 and of the Conahcyt under Grant No. CBF2023-2024-3116. The authors acknowledge useful discussions with Dominique Delande, Thierry Giamarchi, and Nicolas Laflorencie.

APPENDIX: TWO-SPIN DYNAMICS

Let us consider the case of two fermions. In this case, the spin part of the many-body wave function can be written on the snippet basis as $a_1(t)|\uparrow\downarrow\rangle + a_2(t)|\downarrow\uparrow\rangle$, with $a_1(t=0) = 1$ and $a_2(t=0) = 0$. There exists only a hopping term J and the a_i 's obey the differential coupled equations

$$i\hbar\dot{a}_{1,2} = -Ja_{1,2} + Ja_{2,1}. \quad (\text{A1})$$

Taking into account that $a_1^2 + a_2^2 = 1$, then we get

$$\begin{aligned} a_1^2 &= \frac{1}{2} \left\{ 1 + \cos \left[2 \int_0^t J(t') dt' \right] \right\}, \\ a_2^2 &= \frac{1}{2} \left\{ 1 - \cos \left[2 \int_0^t J(t') dt' \right] \right\}. \end{aligned} \quad (\text{A2})$$

The center of mass of each component can be written as

$$\begin{aligned} \bar{x}_{\uparrow} &= \overline{a_1^2 x_1 + a_2^2 x_2}, \\ \bar{x}_{\downarrow} &= \overline{a_2^2 x_1 + a_1^2 x_2}, \end{aligned} \quad (\text{A3})$$

where x_1 and x_2 are the centers of mass of the density distributions ρ_1 and ρ_2 . We observe that

$$\begin{aligned} \bar{x}_{\uparrow} &\simeq \overline{a_1^2} \bar{x}_1 + \overline{a_2^2} \bar{x}_2, \\ \bar{x}_{\downarrow} &\simeq \overline{a_2^2} \bar{x}_1 + \overline{a_1^2} \bar{x}_2. \end{aligned} \quad (\text{A4})$$

Since in the two-particle case $\bar{x}_1 = \bar{x}_{\uparrow}^{\infty}$ and $\bar{x}_2 = \bar{x}_{\downarrow}^{\infty}$, we obtain

$$\bar{x}_{\uparrow,\downarrow} = \frac{1}{2}(\bar{x}_{\uparrow}^{\infty} + \bar{x}_{\downarrow}^{\infty}) \pm \frac{1}{2}(\bar{x}_{\uparrow}^{\infty} - \bar{x}_{\downarrow}^{\infty}) \overline{\cos \left(2 \int_0^t J(t') dt' \right)}. \quad (\text{A5})$$

The J 's distribution not being Gaussian, the disorder average of the cosine function cannot be written in simple terms, and we need to compute it numerically. Indeed, even if \bar{J} determines the spin oscillation frequency, we have verified that the variance σ_j does not allow one to deduce a correct damping time. The comparison between the center-of-mass exact evolution and the approximated one given in Eq. (A5) is shown in Fig. 6.

-
- [1] T. Prat, D. Delande, and N. Cherroret, *Phys. Rev. A* **99**, 023629 (2019).
- [2] L. Tessieri, Z. Akdeniz, N. Cherroret, D. Delande, and P. Vignolo, *Phys. Rev. A* **103**, 063316 (2021).
- [3] R. Sajjad, J. L. Tanlimco, H. Mas, A. Cao, E. Nolasco-Martinez, E. Q. Simmons, F. L. N. Santos, P. Vignolo, T. Macrì, and D. M. Weld, *Phys. Rev. X* **12**, 011035 (2022).
- [4] P. W. Anderson, *Phys. Rev.* **109**, 1492 (1958).
- [5] E. Abrahams, P. W. Anderson, D. C. Licciardello, and T. V. Ramakrishnan, *Phys. Rev. Lett.* **42**, 673 (1979).
- [6] F. Noronha and T. Macrì, *Phys. Rev. B* **106**, L060301 (2022).
- [7] F. Noronha, J. A. S. Lourenço, and T. Macrì, *Phys. Rev. B* **106**, 104310 (2022).
- [8] J. Janarek, B. Grémaud, J. Zakrzewski, and D. Delande, *Phys. Rev. B* **105**, L180202 (2022).
- [9] J. Janarek, D. Delande, N. Cherroret, and J. Zakrzewski, *Phys. Rev. A* **102**, 013303 (2020).
- [10] J. Janarek, J. Zakrzewski, and D. Delande, *Phys. Rev. B* **107**, 094204 (2023).
- [11] D. M. Basko, I. L. Aleiner, and B. L. Altshuler, *Ann. Phys.* **321**, 1126 (2006).
- [12] J. Zakrzewski and D. Delande, *Phys. Rev. B* **98**, 014203 (2018).
- [13] T. Kohlert, S. Scherg, X. Li, H. P. Lüschen, S. Das Sarma, I. Bloch, and M. Aidelsburger, *Phys. Rev. Lett.* **122**, 170403 (2019).
- [14] F. Deuretzbacher, D. Becker, J. Bjerlin, S. M. Reimann, and L. Santos, *Phys. Rev. A* **90**, 013611 (2014).
- [15] L. Yang, L. Guan, and H. Pu, *Phys. Rev. A* **91**, 043634 (2015).
- [16] L. Yang and H. Pu, *Phys. Rev. A* **94**, 033614 (2016).
- [17] G. Pecci, P. Vignolo, and A. Minguzzi, *Phys. Rev. A* **105**, L051303 (2022).
- [18] M. Ljubotina, M. Žnidarič, and T. Prosen, *Phys. Rev. Lett.* **122**, 210602 (2019).
- [19] E. Ilievski, J. De Nardis, M. Medenjak, and T. Prosen, *Phys. Rev. Lett.* **121**, 230602 (2018).
- [20] J. De Nardis, M. Medenjak, C. Karrasch, and E. Ilievski, *Phys. Rev. Lett.* **123**, 186601 (2019).
- [21] D. Wei, A. Rubio-Abadal, B. Ye, F. Machado, J. Kemp, K. Srakaew, S. Hollerith, J. Rui, S. Gopalakrishnan, N. Y. Yao *et al.*, *Science* **376**, 716 (2022).
- [22] A. G. Volosniev, D. V. Fedorov, A. S. Jensen, M. Valiente, and N. T. Zinner, *Nat. Commun.* **5**, 5300 (2014).

- [23] J. Decamp, P. Armagnat, B. Fang, M. Albert, A. Minguzzi, and P. Vignolo, *New J. Phys.* **18**, 055011 (2016).
- [24] R. E. Barfknecht, A. Foester, and N. T. Zinner, *Sci. Rep.* **9**, 15994 (2019).
- [25] M. Griniasty and S. Fishman, *Phys. Rev. Lett.* **60**, 1334 (1988).
- [26] M. Schreiber, S. S. Hodgman, P. Bordia, H. P. Lüschen, M. H. Fischer, R. Vosk, E. Altman, U. Schneider, and I. Bloch, *Science* **349**, 842 (2015).
- [27] K. A. Matveev, *Phys. Rev. B* **70**, 245319 (2004).
- [28] F. Deuretzbacher, D. Becker, and L. Santos, *Phys. Rev. A* **94**, 023606 (2016).
- [29] F. Alet and N. Laflorencie, *C. R. Phys.* **19**, 498 (2018).
- [30] D. J. Luitz, N. Laflorencie, and F. Alet, *Phys. Rev. B* **91**, 081103(R) (2015).
- [31] N. Laflorencie and H. Rieger, *Phys. Rev. Lett.* **91**, 229701 (2003).
- [32] N. Laflorencie and H. Rieger, *Eur. Phys. J. B* **40**, 201 (2004).
- [33] N. Laflorencie, H. Rieger, A. W. Sandvik, and P. Henelius, *Phys. Rev. B* **70**, 054430 (2004).
- [34] N. Laflorencie, *Phys. Rev. B* **72**, 140408(R) (2005).